Terahertz Cavity Magnon Polaritons

T. Elijah Kritzell, Andrey Baydin,* Fuyang Tay, Rodolfo Rodriguez, Jacques Doumani, Hiroyuki Nojiri, Henry O. Everitt, Igor Barsukov,* and Junichiro Kono*

Hybrid light–matter coupled states, or polaritons, in magnetic materials have attracted significant attention due to their potential for enabling novel applications in spintronics and quantum information processing. However, most magnon-polariton studies in the strong coupling regime to date have been carried out for ferromagnetic materials with magnon excitations at gigahertz frequencies. Here, strong resonant photon–magnon coupling at frequencies above 1 terahertz is investigated for the first time in a prototypical room-temperature antiferromagnetic insulator, NiO, inside a Fabry–Pérot cavity. The cavity is formed by the crystal itself with a thickness adjusted to an optimal value. Terahertz time-domain spectroscopy measurements in magnetic fields up to 25 T reveal the evolution of the magnon frequency through Fabry–Pérot cavity modes with photon–magnon anticrossing behavior, demonstrating clear vacuum Rabi splittings exceeding the polariton linewidths. These results show that NiO is a promising platform for exploring antiferromagnetic spintronics and cavity magnonics in the terahertz frequency range.

1. Introduction

Strong resonant coupling of photons and magnons is expected to lead to novel device applications for spintronics, quantum transduction, and quantum information processing.[1–4] Strong photon–magnon coupling was first demonstrated in ferrimagnets and ferromagnets placed inside microwave cavities.[5–7] Since then, many different types of applications of strong photon–magnon coupling have been proposed.[8] However, theoretical and experimental studies on strong photon–magnon coupling in antiferromagnets (AFMs) have been limited although, compared with ferromagnetic materials, AFMs are insensitive to external magnetic perturbations, do not generate stray fields, and exhibit ultrafast dynamics.[9,10] Due to the high frequencies of antiferromagnetic resonances, AFM-based devices can operate in the terahertz (THz) frequency range, which fills the gap between electronics and photonics. THz radiation holds promise for spintronic applications. For example, efficient metallic spintronic emitters have been developed to generate ultrabroadband THz radiation,[11] enabling novel spin-current generation techniques. Moreover, the coupling of THz light with nanometer-wavelength magnon modes through spin-orbit torque offers opportunities for manipulating THz radiation in the field of magnonics.[12] Such advances expand the horizons of spin-based technologies beyond the limitations of gigahertz ranges.

To date, several studies have shown strong photon–magnon coupling, demonstrating vacuum Rabi splittings larger than the linewidths of the lower and upper polariton peaks, for antiferromagnetic resonances.[13–20] However, the studied AFMs either possessed sub-THz magnon frequencies,[13,15,17,20] or required low temperatures,[13,16,18,20] high magnetic fields,[19] or hybridiza-

T. E. Kritzell, A. Baydin, F. Tay, J. Doumani, H. O. Everitt, J. Kono
Department of Electrical and Computer Engineering
Rice University
Houston, TX 77005, USA
E-mail: baydin@rice.edu; kono@rice.edu

T. E. Kritzell, F. Tay, J. Doumani
Applied Physics Graduate Program, Smalley–Curl Institute
Rice University
Houston, TX 77005, USA

A. Baydin, H. O. Everitt, J. Kono
Smalley–Curl Institute
Rice University
Houston, TX 77005, USA

R. Rodriguez, I. Barsukov
Physics and Astronomy
University of California
Riverside, CA 92521, USA
E-mail: igorb@ucr.edu

H. Nojiri
Institute for Materials Research
Tohoku University
Sendai 980-8577, Japan

H. O. Everitt
DEVCOM Army Research Laboratory-South
Houston, TX 77005, USA

H. O. Everitt, J. Kono
Department of Physics and Astronomy
Rice University
Houston, TX 77005, USA

J. Kono
Department of Material Science and NanoEngineering
Rice University
Houston, TX 77005, USA

ADVANCED
SCIENCE NEWS

www.advancedsciencenews.com

ADVANCED
OPTICAL
MATERIALS

www.advopticalmat.de

tion with other collective excitations.[14] Most of these demonstrations have been made in rare-earth orthoferrites,[1,21] in which antiferromagnetic resonances have low damping. Among other AFMs, NiO is a prototypical easy-plane AFM[22] with a high Néel temperature of 525 K; this material has recently gained particular interest due to a series of studies showing current-induced magnetic switching,[23–25] optical control of spin oscillations,[26] non-linear spin response,[27] and the interplay between charge and spin dynamics.[28] The Gilbert damping factor of NiO's antiferromagnetic resonance at $\approx$ 1 THz can be as low as 2.1×10^{-4},[29] which is comparable to that of yttrium iron garnet and is thus suitable for strong photon–magnon coupling realization.[30]

2. Experimental Section

Here, we investigated two single-crystal wafers of NiO, via THz time-domain spectroscopy (THz-TDS) in high magnetic fields up to 25 T.[31–33] We showed that only two magnon modes, at 0.13 and 1 THz, are infrared-active and have two-lobe symmetry with respect to the polarization of the THz excitation beam for both the (110)- and (111)-oriented samples. The magnetic field dependence of the frequency of the 1 THz mode was superlinear, consistent with the two-sublattice model.[9] Furthermore, we observed anticrossing between the 1 THz magnon mode and several Fabry–Pérot (FP) cavity photonic modes by sweeping the magnetic field. These results demonstrate strong photon–magnon coupling at room temperature, and therefore, are promising for developing devices for THz spintronics and quantum information processing applications.

NiO is an easy-plane AFM. Below the Néel temperature, the spins of the Ni^{2+} ions order parallel within each of the {111} planes, as shown in **Figure 1a**. The spins can align along one of the three axes: $\langle 11\bar{2} \rangle$, $\langle 1\bar{2}1 \rangle$, $\langle \bar{2}11 \rangle$ due to magnetic anisotropy. In addition to theoretical studies,[34,35] there have been several experimental reports on antiferromagnetic magnons in NiO studied by time-resolved Faraday rotation, THz-TDS, Raman, and Brillouin scattering measurements. In total, five magnon modes have been observed using different techniques. Two high-frequency antiferromagnetic resonances have been confirmed by Raman scattering,[36] while three lower-frequency antiferromagnetic resonances had been confirmed by Brillouin scattering.[37,38] Far-infrared optical absorption measurements have also confirmed the existence of the 1 THz mode.[39–43] Most recently, Kohmoto et al. have employed optical pump-probe spectroscopy experiments with a circularly polarized pump beam and a Faraday rotation probe beam to observe three magnon modes at about 1.3, 1.1, and 0.1 THz, respectively. They also found a narrow absorption line at 1.1 THz and a broad absorption line at 0.5 THz using THz-TDS down to low temperatures.[44]

In order to explain the existence of these five magnon modes, an eight-sublattice model has been proposed.[38] The magnetic field dependence of some of these modes has been investigated by Brillouin scattering[46] and time-resolved Faraday rotation measurements[47] to refine the parameters used in the eight-sublattice model further. The Brillouin scattering data are limited to the three lowest-frequency modes and magnetic fields up to 7 T, while time-resolved Faraday rotation data have provided the magnetic field-induced evolution of the 1 THz mode up to 10 T in a limited spectral range. Despite these insights into the spin
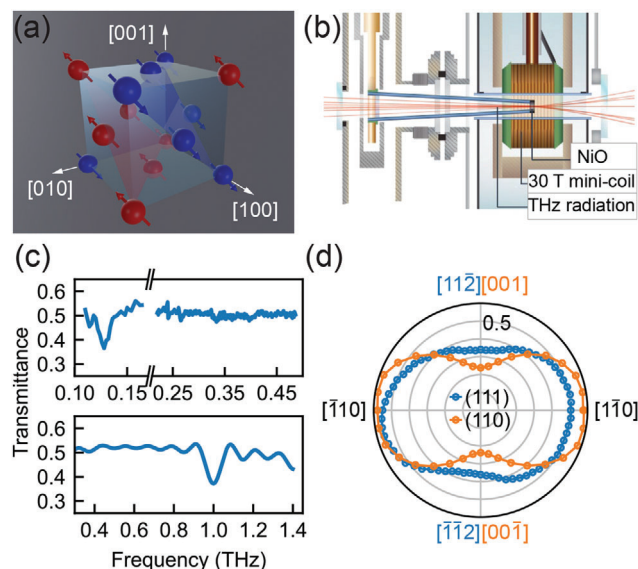

Figure 1. a) Ni^{2+} ion arrangement in the NiO crystal, showing their spin orientations. Oxygen ions are not shown. b) Schematic diagram of the THz time-domain spectroscopy setup in high magnetic fields (RAMBO).[31] c) Transmittance spectra for the (111) NiO crystal obtained using a separate THz ellipsometer[45] [Top] and the THz-TDS setup [bottom]. d) Excitation anisotropy for the 1 THz magnon mode as a function of the magnetic field component of the THz beam, for the (111)- and (110)-cut NiO crystals.

dynamics of NiO, various discrepancies between the model and experimental data[46,47] have been reported, thus calling upon an extension of the experimental data set.

Each single crystal NiO wafer was 10 mm in diameter and 491 um in thickness, cut along the (110) and (111) planes, respectively. The wafers were purchased from SurfaceNet GmbH. We characterized them using x-ray diffraction and x-ray photoelectron spectroscopy to confirm their quality (see Supporting Information). To probe the magnetic field dependence of the magnons and photon–magnon coupling in NiO, a single-shot THz-TDS system was utilized, coupled with a table-top pulsed magnet with a peak field strength of 30 T – the Rice Advanced Magnet with Broadband Optics (RAMBO)[31–33] (see Figure 1b. In THz-TDS, a 775 nm optical pulse from an amplified Ti:Sapphire laser was used (150 fs, 1 kHz, 0.8 mJ, Clark-MXR, Inc., CPA-2001) for the generation and detection of THz radiation. Our total spectral range of 0.1 - 1.5 THz covered four of the previously reported magnon modes. THz pulses were generated via optical rectification in $LiNbO_3$ and guided to the sample using parabolic mirrors. After going through the sample, the THz pulses were detected via electro-optic sampling in a ZnTe crystal. Single-shot detection of THz pulses was achieved using a reflective echelon and a fast CCD camera.[31–33]

The sample was placed on a cold sapphire rod that could reach temperatures down to 12 K. The three most stable temperatures were used in the cryostat for this analysis so that the reported temperatures are known with high accuracy. The maximum magnetic field used was 25 T. Transmittance spectra below 0.3 THz were obtained using a THz ellipsometer, as detailed in Ref. [45]. Because an in-depth understanding of antiferromagnetic spin dy-

**ADVANCED
SCIENCE NEWS**

www.advancedsciencenews.com

**ADVANCED
OPTICAL
MATERIALS**

www.advopticalmat.de

namics was required for employing AFMs in spin-torque devices and other spintronic applications,[48–51] we focus on the behavior of the antiferromagnetic magnon modes and discuss the observed phenomenon of strong photon–magnon coupling.

3. Results and Discussion

Figure 1c shows transmittance spectra for the (111) NiO sample, collected without the magnet, on a large optical aperture to provide the largest spectral bandwidth. Two magnon modes can be clearly identified at 0.13 THz [Top] (taken using THz ellipsometer) and 1 THz [Bottom], respectively. According to these spectra (blue traces), these two modes are the only infrared-active antiferromagnetic resonances. Note that this result is in disagreement with an earlier THz-TDS study of NiO,[44] where a broad absorption line at around 0.5 THz was reported. Although this feature may be absent from our measurements because our sample is thinner (≈0.5 mm vs. ≈5 mm), it must be noted that such broad features may in principle be an artifact arising from setup limitations. We note that in a more recent study utilizing a cw-THz spectrometer,[52] similarly, only the 1 THz magnon mode was observed in the range between 0.4 and 1.25 THz.

Figure 1d shows the measured excitation (absorption) anisotropy for the 1 THz magnon mode for the (111) and (110) NiO crystals. The data were collected at room temperature. The sample was mounted on a motorized rotation stage. For both crystals, we find similar twofold excitation anisotropy. By looking at the magnetic structure [see Figure 1a], we can expect twofold symmetry for the (110)-cut crystal and sixfold symmetry for (111)-cut crystal. The sixfold symmetry expectation can arise because of three equivalent axes of spin alignment, $\langle 11\bar{2}\rangle$, $\langle 1\bar{2}1\rangle$, $\langle \bar{2}11\rangle$. While, for the (110)-cut sample, our data shows clear expected twofold symmetry, the (111)-cut sample exhibits less anisotropy but still a twofold symmetry. A similar twofold anisotropy was also observed in both crystals for the 0.13-THz mode.

NiO has in total 12 orientational domains: four possible $\langle 111\rangle$ stacking directions define twin domains, and per each twin domain there are three $\langle 11\bar{2}\rangle$ spin domains.[53–55] According to a recent second harmonic generation (SHG) study,[55] both coherent and incoherent random assemblies of all twelve orientational domains result in a sixfold SHG signal anisotropy. This leads us to conclude that our sample preferentially consists of fewer than twelve orientational domains.

The data in high magnetic fields have a limited spectral bandwidth compared to the 0 T data, and therefore, we only report the evolution of the 1-THz magnon. **Figure 2a** shows measured absorbance spectra for the (111) NiO sample at different magnetic fields. The 1-THz magnon mode blue-shifts as the magnetic field is increased to about 25 T, which is indicated by the blue dashed line. Figure 2b summarizes the magnetic field dependence of the frequency of this mode, where dashed lines are the fits, as explained below.

The literature values of the effective fields in NiO are $\mu_0 H_E$ = 968.4 T for the exchange field and $\mu_0 H_{HA}$ = 0.635 T and $\mu_0 H_{EA}$ = 0.011 T for the hard-axis ($\langle 111\rangle$) and easy-axis ($\langle 11\bar{2}\rangle$) anisotropies, respectively, while the Landé g-factor $\mathfrak{g}$ = 2.18.[9] Due to the fact that we observe only two infrared-active modes, for simplicity it is sufficient to utilize a two-sublattice model. To as-
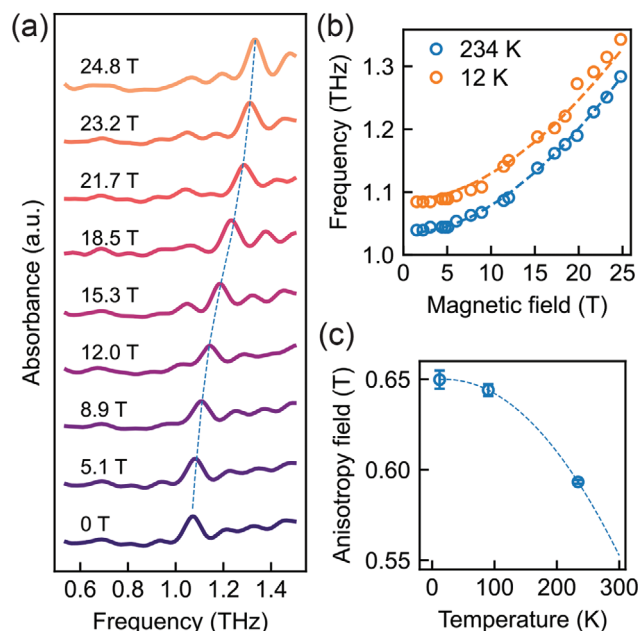

Figure 2. a) Absorbance of (111) NiO as a function of magnetic field at 90 K for several magnetic fields. All traces except the 0 T trace are vertically offset for clarity. The dashed blue line indicates the main feature. b) Magnon frequency as a function of magnetic field at two temperatures. Open circles are from the experimental data, and the super-linear dashed lines are the fits to Equation (1). c) Effective anisotropy as a function of temperature, as derived from fitting data in (b). The dashed line is a guide to the eye.

sess the temperature dependence of magnetic anisotropy in our sample, we estimate the effective anisotropy of the samples using the equation for an easy-plane biaxial AFM frequency[56,57]:

$$\omega/\gamma_r = [2H_E H_A + H_0^2]^{1/2} \tag{1}$$

where $H_A = H_{HA} + H_{EA}$ (magnitude addition) and the external magnetic field H_0 is perpendicular to the easy plane. Because $H_{HA} \gg H_{EA}$, the effective anisotropy is basically the hard-axis anisotropy, i.e., $H_A \approx H_{HA}$. Here, γ_r is the gyromagnetic ratio $\mathfrak{g}\mu_B/\hbar$, where $\mathfrak{g}$ is the Landé g-factor and μ_B is the Bohr magneton.

We fit the magnetic field-dependent magnon frequencies by Equation (1), while fixing the parameters given above and adjusting the effective anisotropy field H_A as the fitting parameter. The effective anisotropy field obtained from this fitting procedure is presented in Figure 2c as a function of temperature. The values of the hard-axis anisotropy are close to those reported in the literature.[9] The temperature dependence of the anisotropy can be approximated by using either the square root of the classical molecular field or the molecular field including biquadratic exchange, as detailed in Ref. [44]. Note that the dashed line in Figure 2c is a guide to an eye and not a fit using the functions mentioned above.

As mentioned above, an eight-sublattice model has been developed and employed recently[47] to describe magnetic field-dynamics of the NiO magnon observed by Brillouin scattering[46] and time-resolved Faraday rotation[47] experiments.

The eight-sublattice model predicts all five modes observed experimentally,[38] and the magnetic field dependence of two upper modes (1.15 THz and 1.29 THz at 0 K) has been calculated.[47] The 1.29-THz mode was shown to change with the magnetic field while the 1.15-THz mode was shown to be magnetic field independent. Wang et al.[47] assigned these two modes to the experimentally observed 1-THz mode, which splits into two as the magnetic field is increased at low temperatures. The authors correlated experimentally observed modes and theoretically predicated modes by their magnetic field dependence, but their frequencies at 0 T were not consistent. It is also important to note that the authors could not resolve the higher-frequency mode at 1.29 THz at low temperatures (previously observed in Raman scattering) due to their frequency bandwidth.[47] A more recent report[58] has also commented on the inapplicability of this model to explain their magnetic field dependent data. Thus, our experimental data provides experimental evidence to investigate the magnetic structure of NiO further and revise the generally accepted eight-sublattice model.

Now, we focus on strong coupling between FP cavity modes and the high-frequency (≈ 1 THz) magnon mode. A FP cavity represents the simplest cavity structure formed by two interfaces. Instead of placing materials under study in between two mirrors, a slab of material in vacuum will act as a FP cavity itself. Thus, when the light wavelength is comparable to the thickness of such a slab, FP fringes (i.e., FP cavity modes) can be easily observed; (see **Figure 3b**). In conventional THz-TDS data analysis, where the FP contributions are intentionally removed from spectra by cutting the time-domain waveform before back-reflection signals appear[59]; e.g., the absorbance shown in Figure 2a was calculated after such a process. Here, however, we calculate transmittance by using the full range of the time domain signal that includes several back reflections; see Figure 3a. The resulting transmittance is shown in Figure 3b. The spacing between the FP cavity modes is 89 GHz, and their full width at half maximum (FWHM) is 28 GHz. For the thickness of the present sample, 491 μm, the magnon and FP cavity modes are detuned at zero magnetic field and room temperature.

Figure 3c shows a transmittance color map as a function of frequency and magnetic field. As the magnon mode frequency increases with the magnetic field, it goes through three FP cavity modes in the measured frequency range. In total, three anticrossings are observed, which indicate formation of cavity magnon polaritons and, therefore, strong photon–magnon coupling. Note that the frequency of the FP cavity mode can be adjusted by changing the sample thickness, allowing for strong photon-magnon coupling to occur at 0 T. The photon-magnon coupling strength g can be estimated from the eigenfrequencies of the quantum Langevin equations[60]:

$$\omega_\pm = \frac{1}{2}(\omega + \omega_{cav}) - \frac{i(\gamma + \kappa)}{4} \pm \sqrt{g^2 + \left(\frac{i(\kappa - \gamma)}{4} + \frac{(\omega - \omega_{cav})}{2}\right)^2} \tag{2}$$

where $\omega_\pm$ are the lower and upper polariton frequencies, ω is the magnon frequency, ω_{cav} is the FP cavity mode frequency, and γ and κ are the magnon and cavity decay rates, respectively.
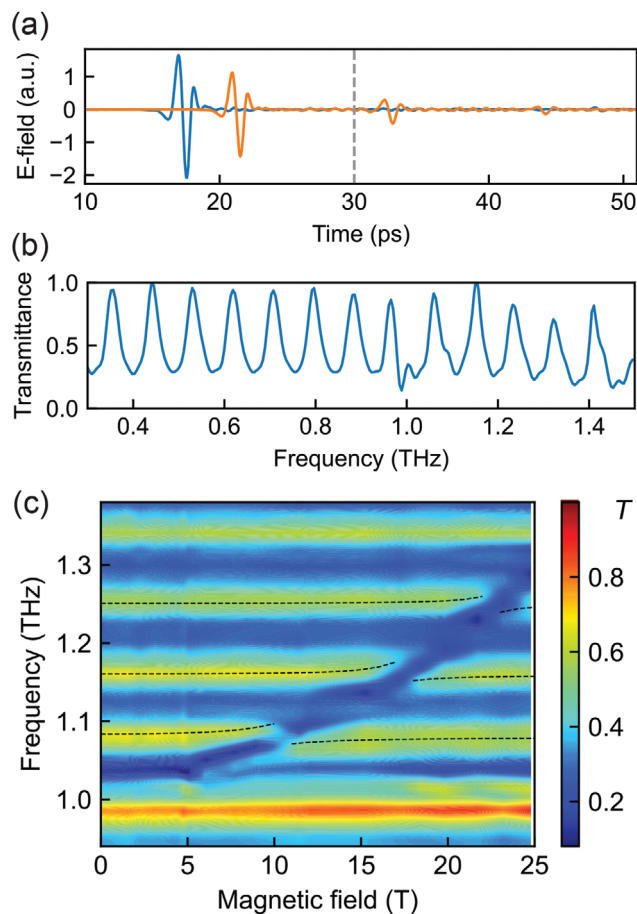

Figure 3. a) THz electric field transmitted through the sample (orange) and an empty aperture (blue). The spectra, including those in Figures 1c and 2a, were obtained through Fourier transform after cutting the time-domain signal before the back reflection (indicated by the gray dashed line). b) Transmittance spectrum obtained from the full THz time-domain trace, at zero magnetic field and room temperature. c) Color map of transmittance as a function of frequency and magnetic field at 234 K, showing anticrossing features between the magnon mode and Fabry–Pérot cavity modes.

The dashed black lines in Figure 3 were calculated by Equation (2) with parameter values of $g = 0.014$ THz, $\gamma = 0.015$ THz, and $\kappa = 0.028$ THz. The value of κ is the FWHM of the FP cavity modes. The value of γ can be estimated from the magnon linewidth in free space. However, since our measured linewidths were instrument limited (25 GHz), we used the literature value of 15 GHz.[52] With these parameter values, we get the cooperativity $C = 4g^2/\gamma\kappa = 1.87$, which satisfies the condition of strong coupling $C > 1$.[61] Note that these values of g and C quantitatively describe the anticrossing behavior of all FP cavity modes shown in Figure 3c and were the same for all temperatures where THz measurements were made (12, 90, and 234 K).

Recently, there has been interest in coupling gigahertz and terahertz magnons in NiO,[62] which was demonstrated via magnetoelastic interaction.[63] Thus, it is interesting to question whether the FP cavity modes can mediate coupling between gigahertz and terahertz magnon modes in NiO. While the two modes are well separated in frequency at the Γ point, they approach each other at

finite wavevector.[9] Therefore, our scheme is promising for the coupling between magnon modes via cavity modes. For example, Białek et al. already demonstrated cavity-mediated coupling of antiferromagnetic magnons in two crystals separated by a well-controlled gap.[64]

4. Conclusion

We studied the temperature and magnetic field dependence of THz antiferromagnetic resonances in NiO and their coupling to FP cavity modes, where the sample itself acted as a cavity. Two infrared-active magnon modes (0.13 and 1 THz) were observed in a broad frequency range, from 0.1 THz to 1.6 THz, with a two-lobed excitation anisotropy with respect to the polarization of the THz pulse. Examining the interactions between the 1 THz magnon mode and FP cavity modes, we observed strong photon–magnon coupling with cooperativity $C = 1.87$ and normalized coupling strength $g/\omega_0 = 0.014$ for the 12$^{\text{th}}$ FP mode. The realization of strong photon–magnon coupling in AFMs in the THz frequency range can bring spintronics and information processing applications to the THz operating regime.

Supporting Information

Supporting Information is available from the Wiley Online Library or from the author.

Conflict of Interest

The authors declare no conflicts of interest.

Data Availability Statement

The data that support the findings of this study are available from the corresponding author upon reasonable request.

[1] X. Li, D. Kim, Y. Liu, J. Kono, *Photonics Insights* **2022**, *1*, 2.

[2] Y.-P. Wang, C.-M. Hu, *J. Appl. Phys.* **2020**, *127*.

[3] D. Lachance-Quirion, Y. Tabuchi, A. Gloppe, K. Usami, Y. Nakamura, *Appl. Phys. Express* **2019**, *12*, 7.

[4] M. Harder, C.-M. Hu, *Solid State Physics*, vol. *69*, chapter Chapter Two - Cavity Spintronics: An Early Review of Recent Progress in the Study of Magnon-Photon Level Repulsion, Elsevier, Amsterdam **2018**, pp. 47–121.

[5] H. Huebl, C. W. Zollitsch, J. Lotze, F. Hocke, M. Greifenstein, A. Marx, R. Gross, S. T. B. Goennenwein, *Phys. Rev. Lett.* **2013**, *111*, 127003.

[6] Y. Tabuchi, S. Ishino, T. Ishikawa, R. Yamazaki, K. Usami, Y. Nakamura, *Phys. Rev. Lett.* **2014**, *113*, 083603.

[7] X. Zhang, C.-L. Zou, L. Jiang, H. X. Tang, *Phys. Rev. Lett.* **2014**, *113*, 156401.

[8] B. Bhoi, S.-K. Kim, in *Solid State Physics*, Vol. *71*, Elsevier, Amsterdam **2020**, pp. 39–71.

[9] S. M. Rezende, A. Azevedo, R. L. Rodríguez-Suárez, *J. Appl. Phys* **2019**, *126*, 151101.

[10] P. Němec, M. Fiebig, T. Kampfrath, A. V. Kimel, *Nat. Phys.* **2018**, *14*, 229241.

[11] T. Seifert, S. Jaiswal, U. Martens, J. Hannegan, L. Braun, P. Maldonado, F. Freimuth, A. Kronenberg, J. Henrizi, I. Radu, E. Beaurepaire, Y. Mokrousov, P. M. Oppeneer, M. Jourdan, G. Jakob, D. Turchinovich, L. M. Hayden, M. Wolf, M. Münzenberg, M. Kläui, T. Kampfrath, *Nat. Photonics* **2016**, *10*, 483.

[12] R. Salikhov, I. Ilyakov, L. Körber, A. Kákay, R. A. Gallardo, A. Ponomaryov, J.-C. Deinert, T. V. A. G. De Oliveira, K. Lenz, J. Fassbender, S. Bonetti, O. Hellwig, J. Lindner, S. Kovalev, *Nat. Phys.* **2023**, *19*, 529.

[13] K. Grishunin, T. Huisman, G. Li, E. Mishina, T. Rasing, A. V. Kimel, K. Zhang, Z. Jin, S. Cao, W. Ren, G.-H. Ma, R. V. Mikhaylovskiy, *ACS Photonics* **2018**, *5*, 1375.

[14] P. Sivarajah, A. Steinbacher, B. Dastrup, J. Lu, M. Xiang, W. Ren, S. Kamba, S. Cao, K. A. Nelson, *J. Appl. Phys.* **2019**, *125*, 213103.

[15] M. Białek, A. Magrez, J.-P. Ansermet, *Phys. Rev. B* **2020**, *101*, 024405.

[16] F. Wu, S. Bao, J. Zhou, Y. Wang, J. Sun, J. Wen, Y. Wan, Q. Zhang, *Nat. Phys.* **2023**, *19*, 1868..

[17] M. Białek, J. Zhang, H. Yu, J.-P. Ansermet, *Phys. Rev. Appl.* **2021**, *15*, 044018.

[18] T. W. J. Metzger, K. A. Grishunin, D. Afanasiev, R. M. Dubrovin, E. A. Mashkovich, R. V. Pisarev, A. V. Kimel, *Appl. Phys. Lett.* **2022**, *121*, 252403.

[19] A. Baydin, K. Hayashida, T. Makihara, F. Tay, X. Ma, W. Ren, G. Ma, G. T. Noe, I. Katayama, J. Takeda, H. Nojiri, S. Cao, M. Bamba, J. Kono, *Phys. Rev. Res.* **2023**, *5*, L012039.

[20] T. G. H. Blank, K. A. Grishunin, A. V. Kimel, *Appl. Phys. Lett.* **2023**, *122*, 072402.

[21] A. M. Balbashov, G. V. Kozlov, A. A. Mukhin, A. S. Prokhorov, *Submillimeter Spectroscopy Of Antiferromagnetic Dielectrics: Rare-Earth Orthoferrites*, World Scientific, Singapore **1995**, pp. 56–98.

[22] T. Schneider, D. Hill, A. Kákay, K. Lenz, J. Lindner, J. Fassbender, P. Upadhyaya, Y. Liu, K. Wang, Y. Tserkovnyak, I. N. Krivorotov, I. Barsukov, *Phys. Rev. B* **2021**, *103*, 144412.

[23] H. Meer, F. Schreiber, C. Schmitt, R. Ramos, E. Saitoh, O. Gomonay, J. Sinova, L. Baldrati, M. Kläui, *Nano Lett.* **2021**, *21*, 114.

[24] P. Zhang, J. Finley, T. Safi, L. Liu, *Phys. Rev. Lett.* **2019**, *123*, 247206.

[25] L. Baldrati, O. Gomonay, A. Ross, M. Filianina, R. Lebrun, R. Ramos, C. Leveille, F. Fuhrmann, T. R. Forrest, F. Maccherozzi, S. Valencia, F. Kronast, E. Saitoh, J. Sinova, M. Kläui, *Phys. Rev. Lett.* **2019**, *123*, 177201.

[26] T. Satoh, S.-J. Cho, R. Iida, T. Shimura, K. Kuroda, H. Ueda, Y. Ueda, B. A. Ivanov, F. Nori, M. Fiebig, *Phys. Rev. Lett* **2010**, *105*, 077402.

[27] S. Baierl, J. H. Metink, M. Hohenleutner, L. Braun, T.-M. Do, C. Lange, A. Sell, M. Fiebig, G. Woltersdorf, T. Kampfrath, R. Huber, *Phys. Rev. Lett.* **2016**, *117*, 197201.

**ADVANCED
SCIENCE NEWS**

www.advancedsciencenews.com

**ADVANCED
OPTICAL
MATERIALS**

www.advopticalmat.de

[28] K. Gillmeister, D. Golež, C.-T. Chiang, N. Bittner, Y. Pavlyukh, J. Berakdar, P. Werner, W. Widdra, *Nat. Commun.* **2020**, *11*, 4095.

[29] T. Kampfrath, A. Sell, G. Klatt, A. Pashkin, S. Mährlein, T. Dekorsy, M. Wolf, M. Fiebig, A. Leitenstorfer, R. Huber, *Nature Photon* **2011**, *5*, 31.

[30] H. Y. Yuan, X. R. Wang, *Appl. Phys. Lett.* **2017**, *110*, 082403.

[31] G. T. Noe, I. Katayama, F. Katsutani, J. J. Allred, J. A. Horowitz, D. M. Sullivan, Q. Zhang, F. Sekiguchi, G. L. Woods, M. C. Hoffmann, H. Nojiri, J. Takeda, J. Kono, *Opt. Express* **2016**, *24*, 30328.

[32] A. Baydin, T. Makihara, N. M. Peraca, J. Kono, *Front. Optoelectron.* **2021**, *14*, 110.

[33] F. Tay, A. Baydin, F. Katsutani, J. Kono, *J. Phys. Soc. Jpn.* **2022**, *91*, 101006.

[34] A. Stevens, *J. Phys. C: Solid State Phys.* **1972**, *5*, 1859.

[35] M. G. Cottam, A. L. Awang, *J. Phys. C: Solid State Phys.* **1979**, *12*, 105.

[36] M. Grimsditch, L. E. McNeil, D. J. Lockwood, *Phys. Rev. B* **1998**, *58*, 14462.

[37] M. Grimsditch, S. Kumar, R. Goldman, *J. Magn. Magn. Mater.* **1994**, *129*, 327.

[38] J. Milano, L. Steren, M. Grimsditch, *Phys. Rev. Lett.* **2004**, *93*, 077601.

[39] H. Kondoh, *J. Phys. Soc. Jpn.* **1960**, *15*, 1970.

[40] M. Tinkham, *J. Appl. Phys.* **1962**, *33*, 1248.

[41] A. J. Sievers, M. Tinkham, *Phys. Rev.* **1963**, *129*, 1566.

[42] R. E. Dietz, G. I. Parisot, A. E. Meixner, *Phys. Rev. B* **1971**, *4*, 2302.

[43] V. V. Pishko, S. L. Gnatchenko, V. V. Tsapenko, R. H. Kodama, S. A. Makhlouf, *J. Appl. Phys.* **2003**, *93*, 7382.

[44] T. Kohmoto, T. Moriyasu, S. Wakabayashi, H. Jinn, M. Takahara, K. Kakita, *J. Infrared Milli Terahz Waves* **2018**, *39*, 77.

[45] T. Hofmann, C. M. Herzinger, A. Boosalis, T. E. Tiwald, J. A. Woollam, M. Schubert, *Rev. Sci. Instrum.* **2010**, *81*, 023101.

[46] J. Milano, M. Grimsditch, *Phys. Rev. B* **2010**, *81*, 094415.

[47] Z. Wang, S. Kovalev, N. Awari, M. Chen, S. Germanskiy, B. Green, J.-C. Deinert, T. Kampfrath, J. Milano, M. Gensch, *Appl. Phys. Lett.* **2018**, *112*, 252404.

[48] R. Rodriguez, S. Regmi, H. Zhang, W. Yuan, P. Makushko, E. A. Montoya, I. Veremchuk, R. Hübner, D. Makarov, J. Shi, R. Cheng, I. Barsukov, *Phys. Rev. Res.* **2022**, *4*, 033139.

[49] A. Etesamirad, R. Rodriguez, J. Bocanegra, R. Verba, J. Katine, I. N. Krivorotov, V. Tyberkevych, B. Ivanov, I. Barsukov, *ACS Appl. Mater. Interfaces* **2021**, *13*, 20288.

[50] I. Barsukov, Y. Fu, C. Safranski, Y.-J. Chen, B. Youngblood, A. M. Gonçalves, M. Spasova, M. Farle, J. A. Katine, C. C. Kuo, I. N. Krivorotov, *Appl. Phys. Lett.* **2015**, *106*, 192407.

[51] A. M. Gonçalves, F. Garcia, H. K. Lee, A. Smith, P. R. Soledade, C. A. C. Passos, M. Costa, N. M. Souza-Neto, I. N. Krivorotov, L. C. Sampaio, I. Barsukov, *Sci. Rep.* **2018**, *8*, 1.

[52] T. Moriyama, K. Hayashi, K. Yamada, M. Shima, Y. Ohya, T. Ono, *Phys. Rev. Mater.* **2019**, *3*, 051402.

[53] M. T. Hutchings, E. J. Samuelsen, *Phys. Rev. B* **1972**, *6*, 3447.

[54] K. Nakahigashi, N. Fukuoka, Y. Shimomura, *J. Phys. Soc. Jpn.* **1975**, *38*, 1634.

[55] I. Sänger, V. V. Pavlov, M. Bayer, M. Fiebig, *Phys. Rev. B* **2006**, *74*, 144401.

[56] A. S. Borovik-Romanov, N. M. Kreines, V. I. Kudinov, *JETP* **1985**, *61*, 801.

[57] A. Safin, S. Nikitov, A. Kirilyuk, V. Tyberkevych, A. Slavin, *Magnetochemistry* **2022**, *8*, 26.

[58] E. Ohmichi, Y. Shoji, H. Takahashi, H. Ohta, *J. Phys. Soc. Jpn.* **2022**, *91*, 095001.

[59] J. Neu, C. A. Schmuttenmaer, *J. Appl. Phys.* **2018**, *124*, 231101.

[60] W. Gao, X. Li, M. Bamba, J. Kono, *Nat. Photonics* **2018**, *12*, 362.

[61] N. M. Peraca, A. Baydin, W. Gao, M. Bamba, J. Kono, in *Semiconductors and Semimetals, Semiconductor Quantum Science and Technology*, Vol *105* (Eds: S. T. Cundiff, M. Kira), Elsevier, Amsterdam **2020**, Ch. 3.

[62] O. Gomonay, D. Bossini, *J. Phys. D: Appl. Phys.* **2021**, *54*, 374004.

[63] D. Bossini, M. Pancaldi, L. Soumah, M. Basini, F. Mertens, M. Cinchetti, T. Satoh, O. Gomonay, S. Bonetti, *Phys. Rev. Lett.* **2021**, *127*, 077202.

[64] M. Białek, W. Knap, J.-P. Ansermet, *Phys. Rev. Appl.* **2023**, *19*, 064007.